Received: 31 January 2018 | Revised: 28 March 2018 | Accepted: 28 May 2018

DOI: 10.1002/joc.5739

International Journal of Climatology RMetS

RESEARCH ARTICLE

Mapping seasonal and annual extreme precipitation over the Peruvian Andes

Fernando Domínguez-Castro[1] | Sergio M. Vicente-Serrano[1] | Juan I. López-Moreno[1] | Kris Correa[2] | Grinia Ávalos[2] | Cesar Azorin-Molina[3] | Ahmed El Kenawy[1,4] | Miquel Tomas-Burguera[5] | Francisco Navarro-Serrano[1] | Marina Peña-Gallardo[1] | Luis Gimeno[6] | Raquel Nieto[6]

[1]Instituto Pirenaico de Ecología, Consejo Superior de Investigaciones Científicas (IPE-CSIC), Zaragoza, Spain

[2]Dirección de Climatología. Servicio Nacional de Meteorología e Hidrología (SENAMHI), Lima, Peru

[3]Regional Climate Group, Department of Earth Sciences, University of Gothenburg, Gothenburg, Sweden

[4]Department of Geography, Mansoura University, Mansoura, Egypt

[5]Estación Experimental de Aula Dei, Consejo Superior de Investigaciones Científicas (IPE-CSIC), Zaragoza, Spain

[6]Environmental Physics Laboratory (EPhysLab), Facultade de Ciencias, Universidade de Vigo, Ourense, Spain

Correspondence
Sergio M. Vicente-Serrano, Instituto Pirenaico de Ecología, Consejo Superior de Investigaciones Científicas (IPE-CSIC), Campus de Aula Dei, P.O. Box 13034, E-50059, Zaragoza, Spain.
Email: svicen@ipe.csic.es

Funding information
European Commission, Grant/Award Number: Water Works 2014 IMDROFLOOD; Ministerio de Educación, Cultura y Deporte; Secretaría de Estado de Investigación, Desarrollo e Innovación, Grant/Award Number: PCIN-2015-220 and CGL2014-52135-C03-01

Seasonal and annual extreme precipitation over the Peruvian Andes have been mapped for the first time. Maps were developed using the most complete, quality-controlled and homogenous daily precipitation records in Peru from 1973 to 2016. For each observed rain gauge series, we defined parameters as the de-clustered daily intensity, total precipitation duration, total magnitude and dry-spell length. Then, we fitted the seasonal and annual series of these variables to a Generalized-Pareto distribution using a peak-over-threshold approach. We estimated the distribution parameters and validated the performance of different thresholds to obtain the best estimation of precipitation probability. We also mapped the distribution parameters obtained for the different meteorological stations using the universal kriging algorithm, accounting for elevation and the distance to the Pacific Ocean as co-variables. The accuracy of the extreme precipitation maps for a period of 25 and 50 years were validated using a jack-knife approach. Some of the maps show strong uncertainty given the random spatial distribution of the variables as a consequence of the complex topography and climate of the region. Nevertheless, the maps show a useful general assessment of the spatial distribution of the precipitation hazard probability over the region, providing a good agreement with the estimations obtained in the meteorological stations for some variables and time periods analysed. Extreme precipitation maps over this high-complex terrain of Peru are of key importance for flood risk assessment, water resources management, crop yield, soil conservation and human settlements.

KEYWORDS

dry spell, extreme precipitation, generalized Pareto distribution, Peru, probability, universal kriging

1 | INTRODUCTION

Extreme precipitation events cause drastic environmental and socioeconomic impacts on local communities in South America (Houston, 2006). Among them, Peru is one of the most vulnerable countries to intense and frequent extreme precipitation events, mainly driven by El Niño-Southern Oscillation (Kane, 1999; Bendix and Bendix, 2006; Seiler *et al.,* 2013). As reported in several studies (e.g., Bendix, 2004; Vilímek *et al.,* 2006; Sulca *et al.,* 2017; Vicente-Serrano *et al.,* 2017), the highly elevated Andes is among the most affected region by these extreme events in Peru. Nonetheless, while numerous studies have analysed the evolution of daily precipitation (e.g., Haylock *et al.,* 2006; Lavado Casimiro *et al.,* 2013; Skansi *et al.,* 2013) and their corresponding atmospheric circulation mechanisms in the

Andes (e.g., Grimm and Tedeschi, 2009; Vicente-Serrano *et al.,* 2017), assessing the probability of occurrence of extreme precipitation events (e.g., wet and dry spells) and their risk and vulnerability maps is markedly lacking in the region.

Daily precipitation data are desired for assessing precipitation hazard probability (Serinaldi and Kilsby, 2014; Madsen *et al.,* 2017) and applying proper statistical approaches (e.g., extreme value theory) to quantify these hazards (Coles, 2001). This is simply because availability of long-term precipitation data at daily resolution allows for estimating data quantiles, which are widely used to define the degree of precipitation hazard in a certain location (Papalexiou *et al.,* 2013). In particular, it is possible to fit the daily precipitation series to a particular probability distribution and employ its corresponding parameters to estimate the probability of occurrence of a certain precipitation value in a period of time or the associated return period.

Nevertheless, although this approach is very useful for risk management and mitigation (Haagenson, 2012; Esteves, 2013; Lawrence *et al.,* 2013), it has certain limitations. Specifically, it only determines the degree of hazard in site-specific locations, that is, where precipitation observations exist. This aspect is crucial in areas of complex topography and atmospheric dynamics as the Andes region, where precipitation is highly variable over space and time, combined with a generally low density of rain gauge observations (Yarleque *et al.,* 2016).

To overcome these limitations, two different approaches have been adopted by many scientists: spatial regionalization according to the calculation of homogeneous regions (e.g., Fitzgerald, 1989; Hosking and Wallis, 2005; Trefry *et al.,* 2005; Serra *et al.,* 2016; Carreau *et al.,* 2017) and spatial interpolation (e.g., Beguería *et al.,* 2009; Mailhot *et al.,* 2013). Nonetheless, these approaches also introduce some uncertainty (Szolgay *et al.,* 2007; Panthou *et al.,* 2015). For example, while regionalization reduces the spatial uncertainty associated with some distribution parameters (Rosbjerg *et al.,* 1992; Naveau *et al.,* 2014), it does not account for the possible smooth variations of these parameters over space, which may be driven by topographic and geographic characteristics. In contrast, spatial interpolation approaches consider spatial uncertainty of the distribution approaches, but allowing the inclusion of auxiliary topographic and geographic variables and thus generating smooth maps of the associated daily precipitation hazard (Cooley *et al.,* 2007; Beguería *et al.,* 2009). Overall, different studies confirmed the capacity of these interpolation techniques to obtain robust maps of daily precipitation hazard in different regions of the world (e.g., Begueria and Vicente-Serrano, 2006; Szolgay *et al.,* 2009; Vicente-Serrano *et al.,* 2009; Blanchet and Lehning, 2010).

The primary objective of this study is to develop, for the first time, probability maps of extreme precipitation for the Andes region of Peru using daily observed precipitation data and spatial interpolation techniques. In comparison to earlier studies worldwide, which focused mostly on precipitation intensity estimation (e.g., Madsen *et al.,* 1994; Cooley *et al.,* 2007; Boessenkool *et al.,* 2017), our study extends further to different precipitation hazard metrics, including: maximum precipitation intensity, magnitude, duration and dry spell length, providing a comprehensive assessment of precipitation hazard in the study domain.

2 | DATASET DESCRIPTION

Daily precipitation data from 370 meteorological stations, spanning the period from 1928 to 2016, were provided by the Servicio Nacional de Meteorología e Hidrología (SENAMHI; http://www.senamhi.gob.pe/; Accessed 1st February 2018) in Peru. The raw data were subjected to quality control checks to remove outliers and erroneous data. With the lack of detailed metadata about observational issues (e.g., changes in station location, observing practices, instruments, surrounding environments, etc.), daily precipitation data were set for homogeneity testing using three relative homogeneity statistics. In particular, we applied the Standard Normal Homogeneity Test for a single break (Alexandersson, 1986), the two-phased regression test (Easterling and Peterson, 1995), and the Vincent method for multiple shifts (Vincen, 1998). The combination of these three tests allowed the detection of not only the most significant break points in each series, but also multiple shifts. To apply these relative tests, composite seasonal and annual reference series were created for each candidate series using data from the best Pearson correlation coefficients ($r > 0.7$) of neighbouring stations. Importantly, to account for the possible impact of complex topography on generating reference series, both reference and candidate series were standardized to have the same average and standard deviation. After detecting inhomogeneities, a monthly correction factor was defined and interpolated to daily data following the approach of Sheng and Zwiers (1998). Finally, a reconstruction procedure was applied to the homogenized series, with the aim of building long-term time series by making a good use of short time series. Herein, it is noteworthy indicating that our robust data processing protocol was applied iteratively to ensure that the final dataset is free from any erroneous data or inhomogeneities that may be introduced to the series by the reconstruction process itself. In this work, we employed daily quality-controlled, homogenized and complete rainfall data from 178 series spanning the period from 1973 to 2016. As illustrated in Figure 1, these stations show a reasonable spatial coverage over the Andes region.

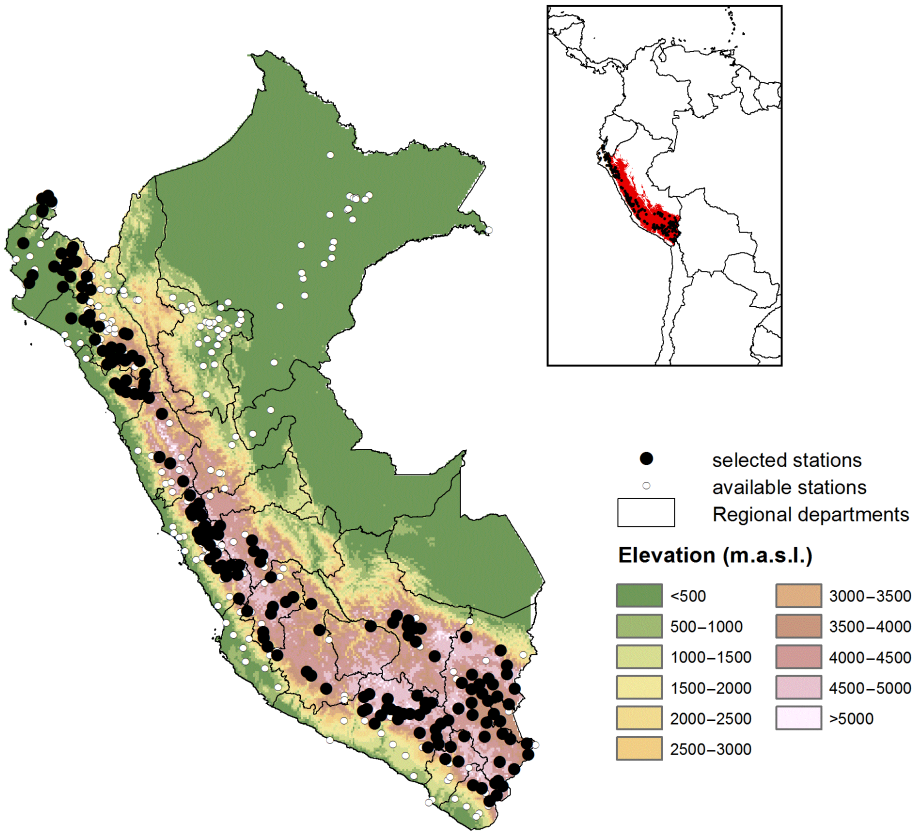

FIGURE 1 Spatial distribution of the meteorological stations across Peru [Colour figure can be viewed at wileyonlinelibrary.com]

3 | METHODS

3.1 | Definition of daily precipitation variables

Hydrological and agricultural hazards can be related to extreme wet and dry events. On the one hand, torrential flooding is usually linked to short and very intense rainfall (Belachsen *et al.,* 2017; Borga *et al.,* 2007; Dullo *et al.,* 2017). On the other hand, regional floods are associated with long-lasting rainfall, irrespective of the precipitation intensity (Saharia *et al.,* 2017). Likewise, consecutive wet days may cause soil saturation and landslides (Crosta, 1998), while agriculture losses, forest fires and ecological damages are usually related to long dry-spells (Barron *et al.,* 2003; Halder *et al.,* 2016). For this reason, we have focused on four precipitation variables obtained from the homogenized precipitation series:

- Rainfall intensity, defined as the maximum daily precipitation for each wet event. Wet events are characterized by consecutive days with daily precipitation higher than 0 mm. This maintains the necessary independence of the precipitation events (Beguería, 2005).
- Rainfall duration, defined as the maximum length of consecutive wet days.
- Rainfall magnitude, defined as the total precipitation magnitude during the duration of each wet event.
- Dry spell length, defined as the maximum length of consecutive days with no precipitation.

The date for rainfall intensity was set for the day of occurrence of the event but the rainfall duration, magnitude and dry spell length were assigned to the last day of the sequence. We computed these variables for each station at annual and seasonal scales. Herein, seasons are defined as: winter (JJA), spring (SON), summer (DJF) and autumn (MAM).

3.2 | Precipitation risk estimation and validation

For each station, we assessed precipitation risk based on the exceedance over threshold approach using the annual and seasonal series of the four variables, according to a threshold (x_0), where:

$$Y = X - x_0 \forall X > x_0. \quad (1)$$

We tested different thresholds based on the centiles computed for each series (i.e., 0th, 10th, 20th,…, 90th and 95th), with the purpose of determining the best centile threshold for defining the exceedance series for rainfall intensity, duration, magnitude as well as dry spell length.

It has been widely demonstrated that the probability distribution of an exceedance series with random occurrence times belongs to the Generalized Pareto distribution (GPA) (e.g., Hosking and Wallis, 1987; Wang, 1991; Pham *et al.,*

2014). The GPA distribution has been widely used to estimate the quantiles of daily precipitation intensity (e.g., Madsen *et al.,* 1998; Begueria and Vicente-Serrano, 2006; Tramblay *et al.,* 2013) as well as dry spell length (e.g., Vicente-Serrano and Beguería-Portugués, 2003; She *et al.,* 2013) based on exceedance series. The GPA distribution is a flexible, long-tailed distribution, whose distribution function is formulated as:

$$F(x)=1-\left[1-\frac{\kappa}{\alpha}(x-\varepsilon)\right]^{1/\kappa}, \quad (2)$$

where κ is the shape parameter, α is the scale parameter and ε is the location parameter or distribution origin that corresponds to the lower bound x_0. The GPA parameters are obtained using the L-moment statistics following Hosking (1990). Hosking (1990) provided parametric approximations of the relationships between τ3 (L-skewness) and τ4 (L-kurtosis), which allows for comparison with the ratio estimations, and accordingly determining the suitability of GPA distribution to fit the exceedance obtained from different x_0 values. As a first approach to determine the suitability of the different x_0 thresholds to obtain exceedance series with good fitting to a GPA distribution, we plotted L-moments for each annual and seasonal series of precipitation variables considering different x_0 thresholds.

To select the most suitable threshold to estimate the quantiles, we compared the observed rainfall intensity, duration, magnitude and dry spell length with those estimated using GPA distribution. For this purpose, we calculated the probability that an event of magnitude X_T in a period of T = 43 years (expressed in the original scale) will occur at least once in a period of t years, according to:

$$X_T=\varepsilon+\frac{\alpha}{\kappa}\left[1-\left(\frac{1}{\lambda T}\right)^{\kappa}\right], \quad (3)$$

where λ is a frequency parameter equalling the average number of occurrences of X per year in the original sample.

The performance of each threshold was assessed by means of three accuracy statistics, including the Mean Absolute Error (MAE), the Willmott's *D* agreement index (Willmott, 1981), and the Pearson's r correlation coefficient.

Once a threshold was established to create the exceedance series of the different variables we determined the goodness of the GPA modelling. For this purpose we used p–p (probability-probability) plots, which indicate how closely the empirical and modelled GPA cumulative distribution functions (cdfs) are. This procedure was applied to the annual and seasonal series of the four variables for the available 178 observatories. Empirical cdfs were obtained using the plotting position formula proposed by Hosking (1990) for highly skewed data, as:

$$P(X\leq x)=\frac{i-0.35}{N}, \quad (4)$$

where *i* is the rank of the observations arranged in an increased order, and *N* is the number of observations. Goodness of agreement between empirical and modelled cdfs was determined by means of the Willmott's *D* agreement index and a weighted correlation coefficient to give more importance to the highest and less frequent observations in the sample, which are of greatest importance in extreme values analysis. The weight was defined using the empirical cdf, as:

$$w_j=\frac{1}{1-cdf(j)}. \quad (5)$$

3.3 | Spatial mapping and validation

To develop spatial maps for precipitation-related hazards, we followed the methodology proposed by Begueria and Vicente-Serrano (2006) with some modifications. The purpose was to interpolate GPA parameters (to obtain return periods, probabilities of extreme events, etc.) at stations, where climatic information is available, to areas with no meteorological data. With the presence of many interpolation algorithms varying from local to global techniques (Burrough and McDonnell, 1998), our preference was given to apply local interpolators that account for the role of covariables (e.g., topography) on the spatial variations of the interpolated parameters. Previous works (e.g., Weisse and Bois, 2002; Vicente-Serrano *et al*., 2003) demonstrate that in mountainous areas and in regions with complex atmospheric influences, such as the Andes of Peru, local interpolators and geostatistical methods that consider external variables give better predictions, with low prediction errors, of spatial variability of climatic variables at different scales. In this study, the GPA distribution parameters were interpolated at a grid spacing of 5 × 5 km by means of the universal kriging method, which includes a trend function defined on the basis of a set of covariates (Pebesma, 2004). In comparison to other methods, this interpolator showed better performance in mapping climate variables over complex terrain regions (Attorre *et al.,* 2007; Hofstra *et al.,* 2008). Here, latitude, longitude, distance to Pacific Ocean and elevation at each grid cell were considered as auxiliary variables. Spherical semivariograms with nugget effect were used to estimate the weights of the different stations, and estimations of error (kriging variance) were also spatially provided.

We used a jackknife cross-validation method to validate the maps of GPA parameters. This method is based on withholding, in turn, one station out of the network, estimating the parameters from the remaining stations and calculating the difference between the predicted and observed value for each withheld station (Phillips *et al.,* 1992). This method has been frequently used in climatology (e.g., Daly *et al.,* 1994; Holdaway, 1996; Hofstra *et al.,* 2008; El Kenawy *et al.,* 2010), particularly in regions with scarce data. The Willmott's agreement index (*D*) was then calculated to compare the observed and interpolated GPA parameters at the points

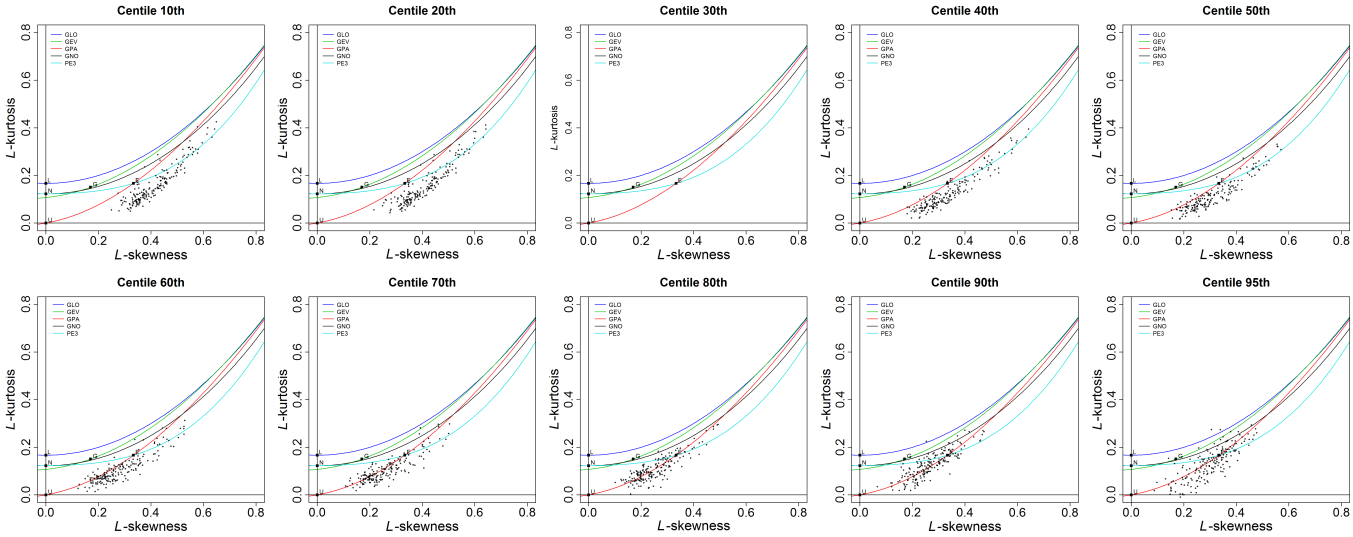

FIGURE 2 L-moment diagrams for de-clustered annual precipitation intensity series over different thresholds [Colour figure can be viewed at wileyonlinelibrary.com]

of the meteorological stations, providing an estimation of the goodness of the spatial interpolation of the different parameters at different timescales (i.e., seasonal and annual) and for the different precipitation variables.

Once we obtained the maps of annual and seasonal parameters, we calculated the probability that an event of magnitude X (expressed in the original scale) will occur at least once in a period of T years, according to:

$$P(X \geq x) = 1 - \left[1 - \left(\kappa \frac{x - x_0}{\propto}\right)^{\left(1/\kappa\right)}\right]^{\lambda t}. \quad (6)$$

Herein, two different periods: short ($T = 25$) and long (T50) were considered for the analysis. Finally, we calculated new accuracy statistics to compare the maximum precipitation estimated in both periods with those obtained at each meteorological station using the calculated GPA parameters.

4 | RESULTS

4.1 | Statistical distribution and threshold selection

Figure 2 shows L-moment statistics for the de-clustered precipitation intensity series obtained for a range of thresholds (from 10th to 95th centiles) using annual precipitation series. Each point represents the parameters calculated in one of the available meteorological stations. Each line represents a theoretical curve distribution that is, generalized logistic (GLO, blue), generalized extreme value (GEV, green), generalized Pareto (GPA, red), generalized normal (GNO, black) and Pearson type III (PE3, light blue). The series of all seasons have been considered here. As noted, the series tend to fit to the theoretical statistics of the GPA distribution, particularly for upper thresholds. A clear example is precipitation intensity series obtained using the 70th centile as threshold, where points distribute closely to the GPA line. At the seasonal

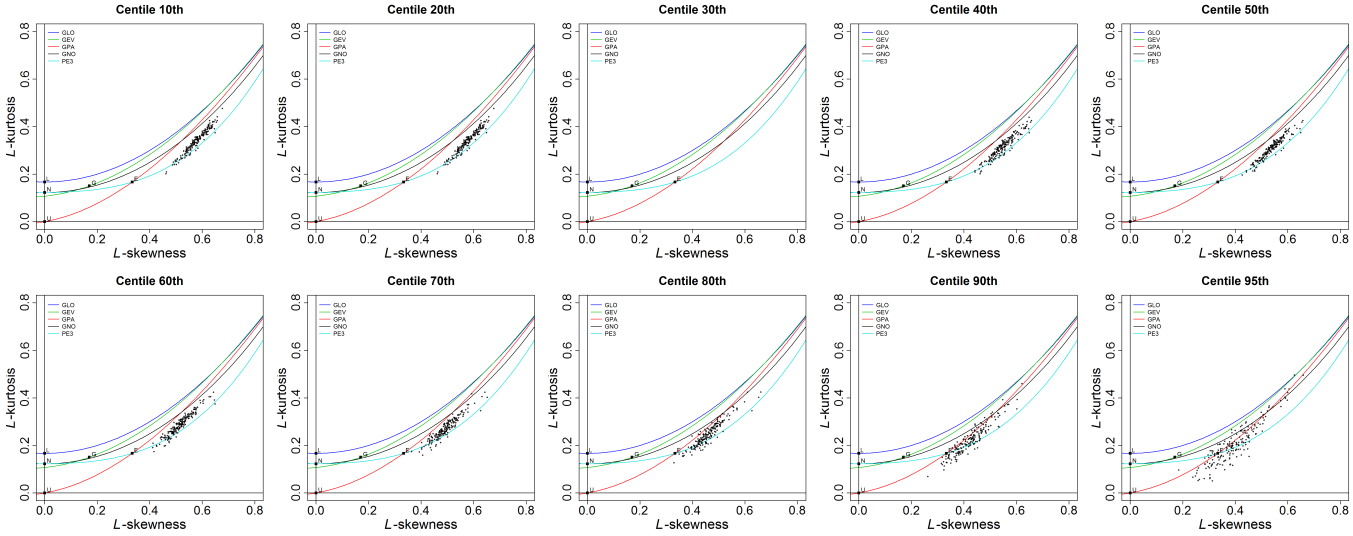

FIGURE 3 As Figure 2, but for annual precipitation duration series [Colour figure can be viewed at wileyonlinelibrary.com]

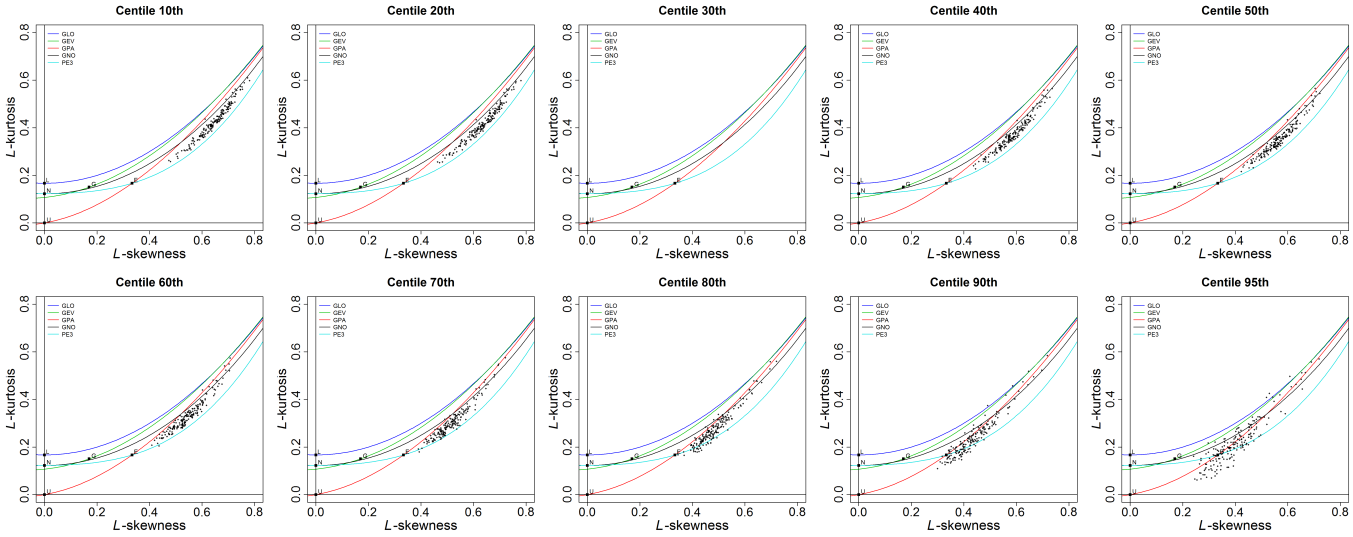

FIGURE 4 As Figure 2, but for annual precipitation magnitude series [Colour figure can be viewed at wileyonlinelibrary.com]

scale (Figures S1 to S4 in Appendix S1, Supporting Information), a similar pattern is observed, but with more dispersion, which can be seen in the context of the lower number of cases in comparison to the annual series. Similar to annual series, it can be noted that –for higher thresholds- the seasonal precipitation intensity series also tend to show statistics closer to those expected by a GPA distribution. However, there is also some dispersion corresponding to upper centiles, as a consequence of the lower length of the seasonal series.

A comparison between precipitation variables indicates that the series of precipitation duration shows lower dispersion in comparison to precipitation intensity series. Nonetheless, they reveal a clear fit to the theoretical L-moments curve of the GPA distribution considering upper centile thresholds (Figure 3). Figures S5–S8 in Appendix S1 suggest some seasonal difference, where there is a greater dispersion from the GPA distribution line for the upper centile thresholds corresponding to winter and spring seasons.

Precipitation magnitude series show a similar pattern both annually (Figure 4) and seasonally (Figures S9 to S12 in Appendix S1). In general, the points follow the theoretical line of the GPA distribution, mostly considering upper centiles to define the thresholds. Similar results are found for dry spell series (Figure 5 and Figures S13 to S16 in Appendix S1). Taking all these results together, it can be confirmed that all variables that characterize daily precipitation in the Andean region show good agreement between L-moment parameters and those expected following the GPA distribution.

The different L-moment diagrams suggest the selection of high centile thresholds to obtain the series of precipitation intensity, duration, magnitude and dry spell length. This finding is confirmed when comparing the seasonal and

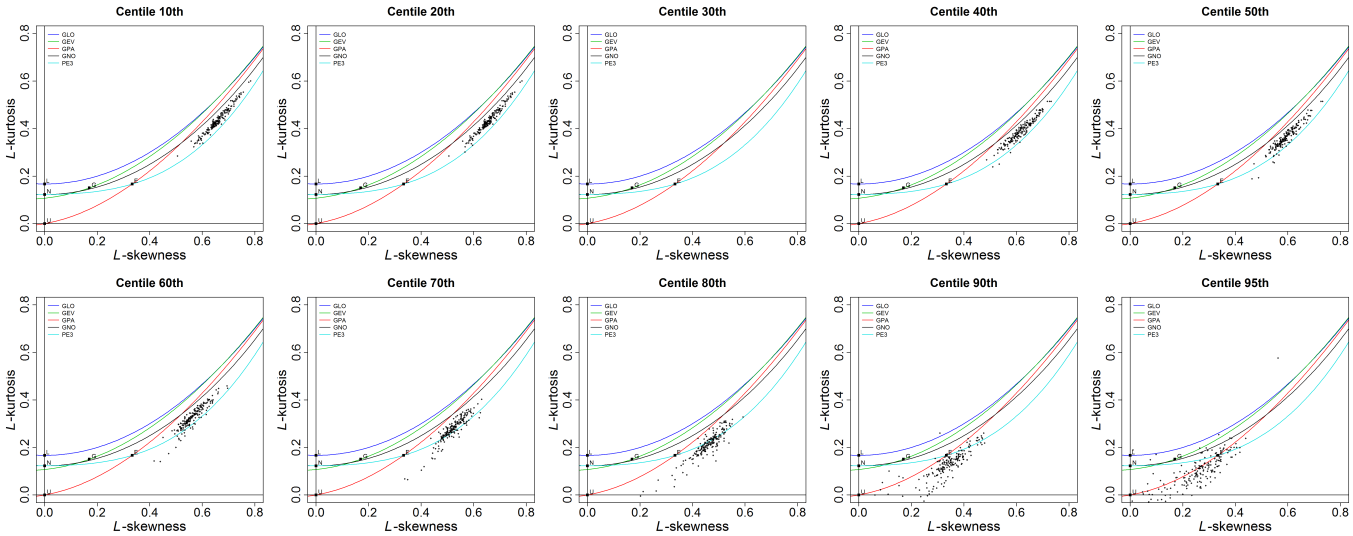

FIGURE 5 As Figure 2, but for annual precipitation dry spell length series [Colour figure can be viewed at wileyonlinelibrary.com]

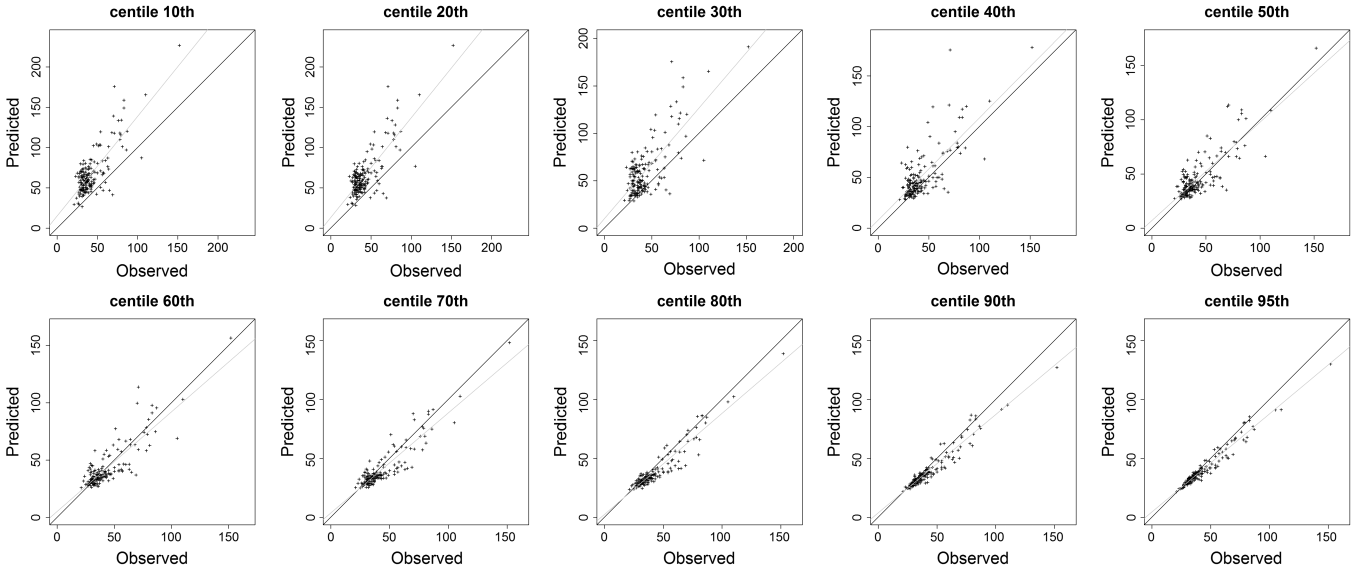

FIGURE 6 Relationship between observed and predicted maximum precipitation intensity (annual) for 1973–2016 using the Generalized Pareto Distribution and series obtained at different thresholds

annual maximum observed values of the four variables over the study period, as predicted by means of the calculated parameters of the GPA distribution. Figures 6–9 show the comparison between maximum observed and predicted values considering the annual series, while the results corresponding to seasonal series are depicted in Figures S17 to S32 in Appendix S1. As noted, the threshold corresponding to low centiles do not coincide between observed and predicted maximum values for all variables. In general, there is a clear overestimation of observations, particularly for dry spell series. On the contrary, there is a high agreement between the observed and predicted maximum values for all variables, considering thresholds above the 90th centile. Different accuracy statistics (Willmott's *D*, MAE and Pearson's r coefficients) to assess the overall agreement between observed and predicted precipitation variables for both seasonal and annual series are summarized in Figure 10. Apart from precipitation duration and magnitude that shows weak agreement between observed and predicted values in summer, the rest of variables reveal a general good agreement between observations and predictions. Again, the skill of predictions in reproducing observed maximum values is improved markedly when considering upper centiles. Higher (lower) *D* and Pearson's r (MAE) values are obtained considering high centiles to obtain the peaks-over-threshold (POT) series. Independently of the variable or the timescale (i.e., seasonal vs. annual), the best agreement is obtained using the 90th and 95th centile thresholds. As expected, a better performance is found for the annual series, in comparison to the seasonal series, as a consequence of the increase in the sample size. Specifically, the seasonal series do not show a clear signal, although -in all cases- the accuracy

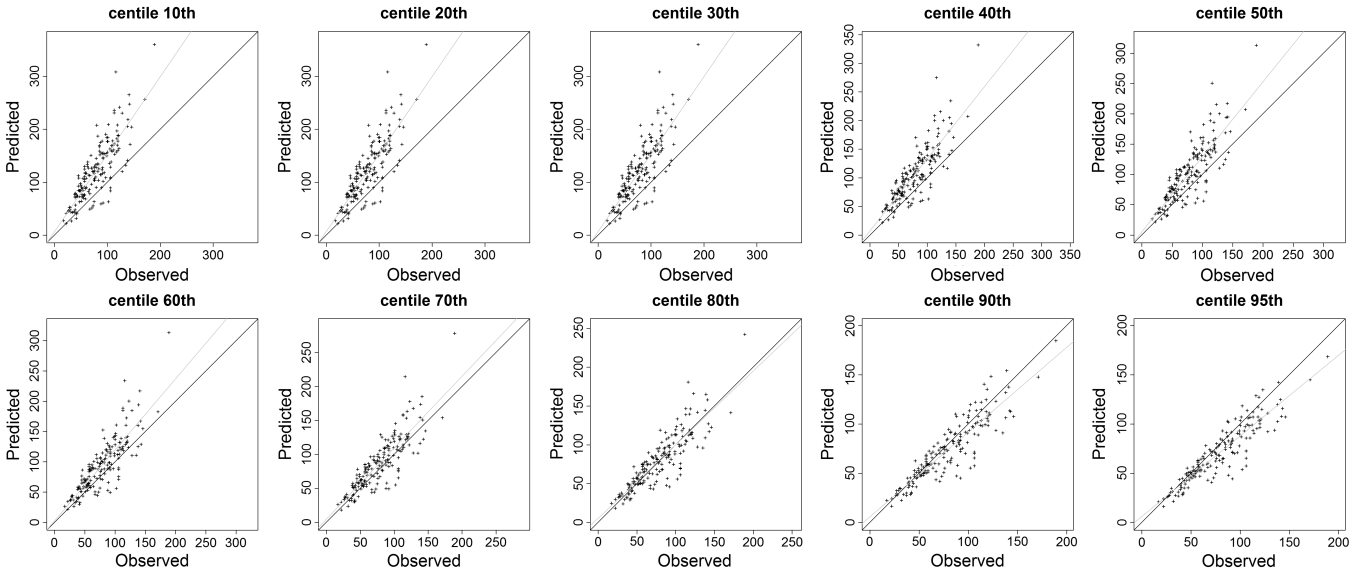

FIGURE 7 As Figure 6, but for maximum annual precipitation duration

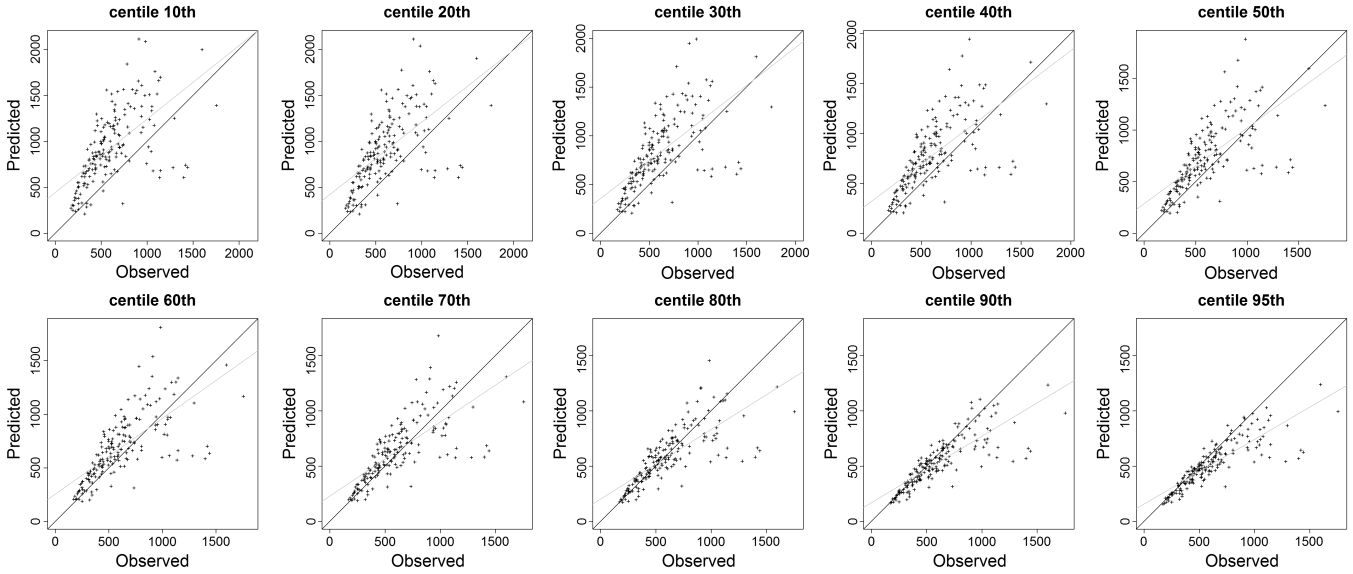

FIGURE 8 As Figure 6, but for maximum annual precipitation

statistics recommend the use of high centiles to select the POT series. Taking these findings together, we decided to choose the 90th centile as a threshold to develop the POT series and in turn make the different estimations. This selection will maintain a sufficient sample size to make robust calculations considering a high centile as threshold. An exploratory analysis indicates that using higher centiles (e.g., the 95th centile) will not secure a statistically appropriate sample size to get reliable estimations (Table S1 in Appendix S1).

4.2 | At-site performance of statistical model

We assess the skill of the POT series, created using the 90th centile, and the GPA distribution in determining the cumulative distribution function (cdf) for the four precipitation variables (i.e., intensity, duration, magnitude and dry spell length. Figure 11 shows an example of the relationship between the empirical and modelled cdfs, computed for the annual series of all precipitation variables in *Granja Porcon* station. As noted, there is a strong agreement between empirical and modelled cdfs, demonstrating that the definition of the POT series using GPA distribution and a 90th centile is an appropriate choice to identify the probability of occurrence of an event in this station, regardless of intensity, duration, magnitude or a dry spell of certain duration. This finding is confirmed for all meteorological stations. Table 1 summarizes the mean and standard deviation for weighted correlation and Willmott's *D* index averaged for all meteorological stations in the Andes. Results suggest that predicted cdf using the GPA distribution and the 90th centile to define the POT series are very close to the observed cdf. This finding is confirmed for both seasonal and annual series, with

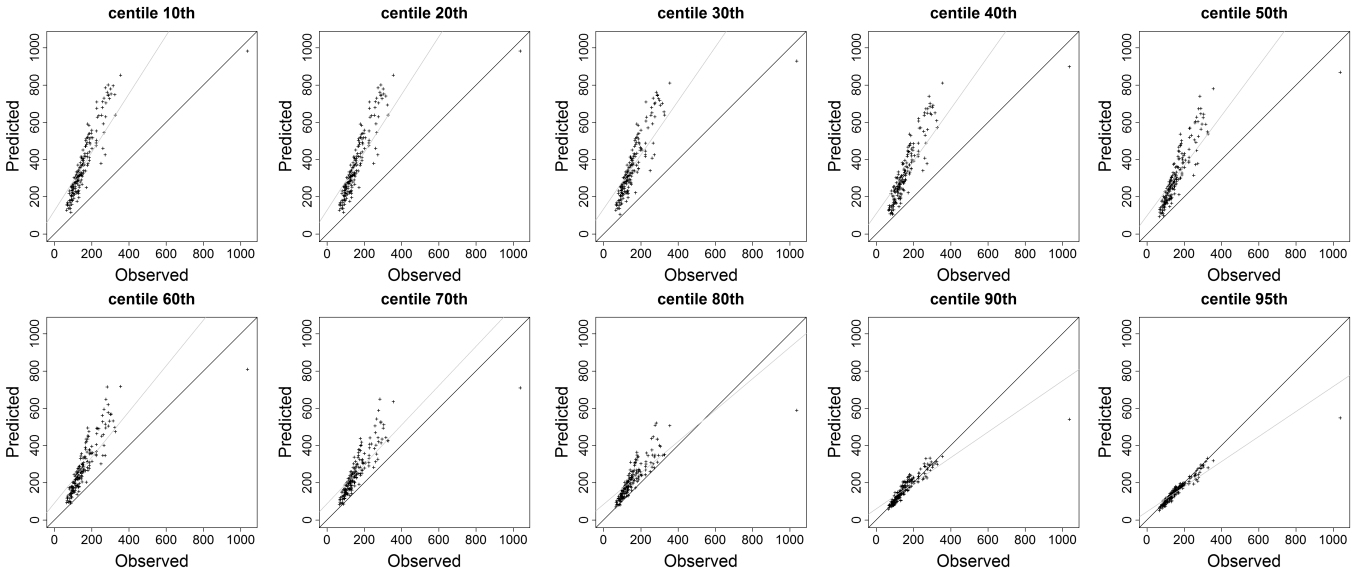

FIGURE 9 As Figure 6, but for maximum annual precipitation dry spell length

mean weight correlations being generally higher than 0.99 with very low standard deviations, and similar results for Willmott's D value. Moreover, given that weighted correlation has a higher influence on the performance of high events, which are more relevant to hazard estimations, it provide additional indicator on the robustness of the methodology used to determine probabilities for extreme precipitation events (Table 1).

4.3 | Mapping generalized Pareto parameters

Figure 12 presents an example of mapping three parameters of the GPA distribution (x_0, α and κ) and the λ statistic for the annual and seasonal precipitation intensity series. The spatial variance of the estimations is also mapped. Results reveal important spatial and seasonal differences among the four parameters. For some parameters (e.g., x_0 and λ), there are gradual transitions at the annual and seasonal scales and dominant spatial gradients between the regions close to the Pacific Ocean and the regions close to the Amazonian area. In contrast, the spatial patterns of α and κ show more differences, with no clear spatial gradients. This pattern is observed at the annual and seasonal scales. The variance also shows dominant spatial gradients, informing on the uncertainty corresponding to estimations. Lower variances are found for λ, suggesting low uncertainty in mapping this parameter across the study region. For x_0, α and κ, variance is much higher, mostly in the northeastern region, where the uneven distribution of stations can be responsible for the higher uncertainty of estimations. Nonetheless, there are important seasonal differences. One example is x_0, which shows higher variance in summer than in winter. The opposite is noted for α, where a complex spatial pattern is found in winter. Figures S33 to S35 in Appendix S1 show the spatial distribution of the GPA parameters for precipitation duration, magnitude and dry spell length over the study domain. Results indicate important differences in the spatial gradients as well as the variability of the mapped parameters. Notably, there are clear spatial gradients, with a southwest-northeast dipole, particularly for the parameters of dry spell length. Table 2 summarizes Willmott's D statistics obtained using the jackknife approach for the GPA parameters, besides λ statistic, estimated annually and seasonally from the four variables. Table 2 shows varying performance among the spatial models, as a function of the GPA parameter, precipitation variable and the timescale (seasonal

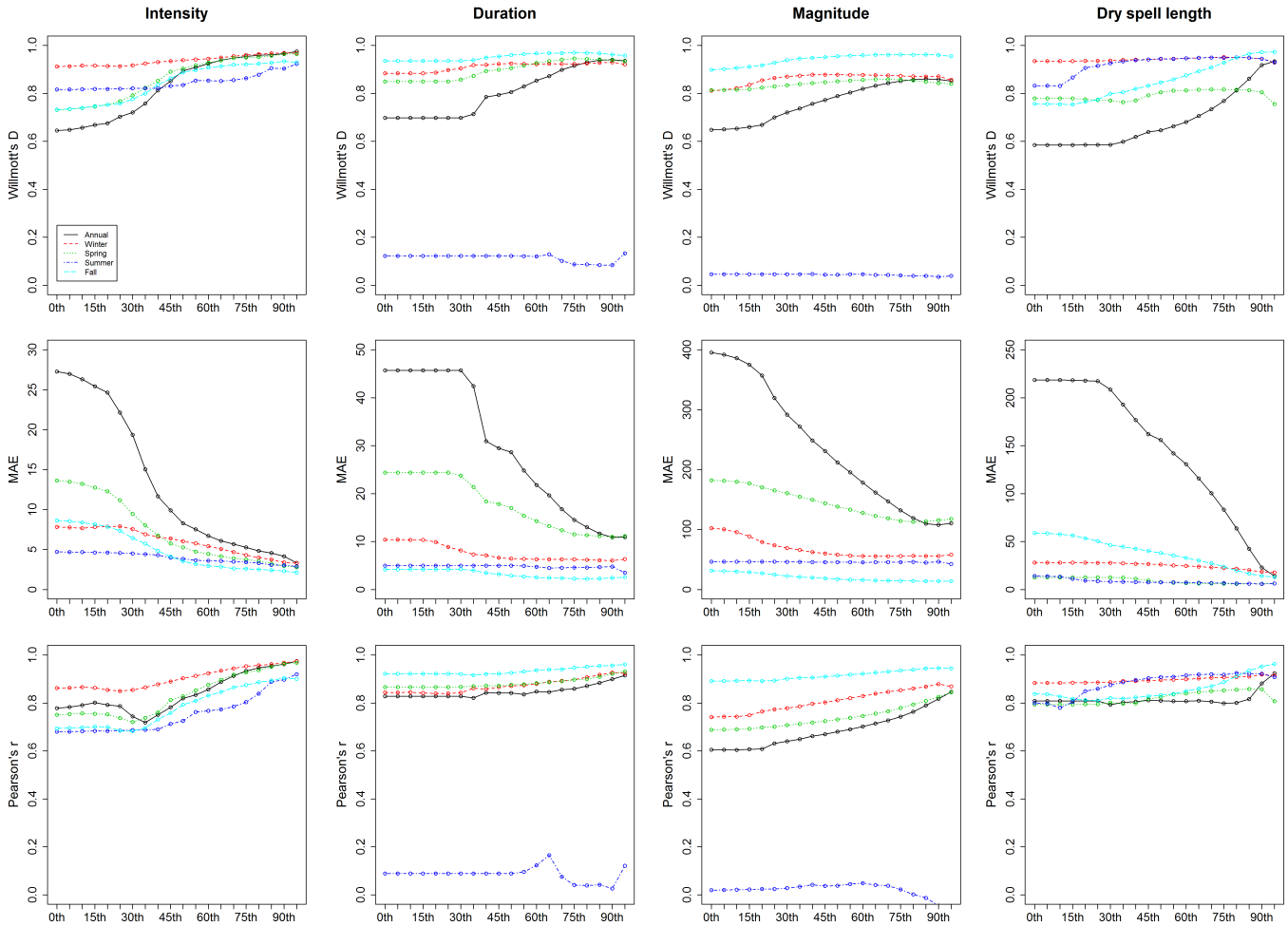

FIGURE 10 Error/accuracy statistics between observed and predicted precipitation intensity, duration, magnitude and dry spell length at the annual and seasonal scales considering the series of POT for the different variables obtained at different centiles [Colour figure can be viewed at wileyonlinelibrary.com]

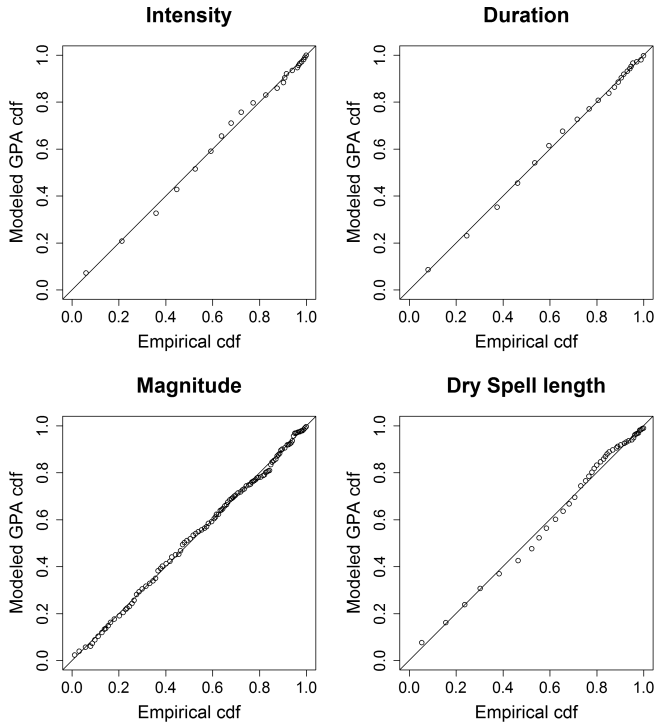

FIGURE 11 Example of probability-probability plot between observed and predicted cdfs for the annual intensity, duration, magnitude and dry spell length series obtained at a threshold of 90th centile in the station "Granja Porcon"

vs. annual). In general, we find lower D values for α and κ than for x_0 and λ, but with some exceptions found for the dry spell length, which shows higher D values for κ and α parameters considering the annual and seasonal series. The high spatial variability of κ corresponds to low D values for the shorter seasonal series as well as the longer annual series. Generally, D values obtained for κ for the different variables are higher than those of α. Figures S36 to S55 in Appendix S1 illustrate the relationship between the estimated GPA parameters ($+\lambda$) at the seasonal and annual scale for the different variables and those predicted using kriging method by means of the jack-knife approach.

4.4 | Hazard mapping and validation

Figures 13–16 depict the spatial distribution of the expected maximum precipitation intensity, duration, magnitude and dry spell length at the annual and seasonal scales for a period of 25 and 50 years. As illustrated in Figure 13, maximum precipitation intensity shows noticeable spatial and seasonal contrasts with estimated higher precipitation intensity over the northwestern region. Notably, the maximum precipitation intensity expected within 50 years is higher than 70 mm, mostly corresponds to summer and autumn. Winter and spring seasons show expected lower maximum

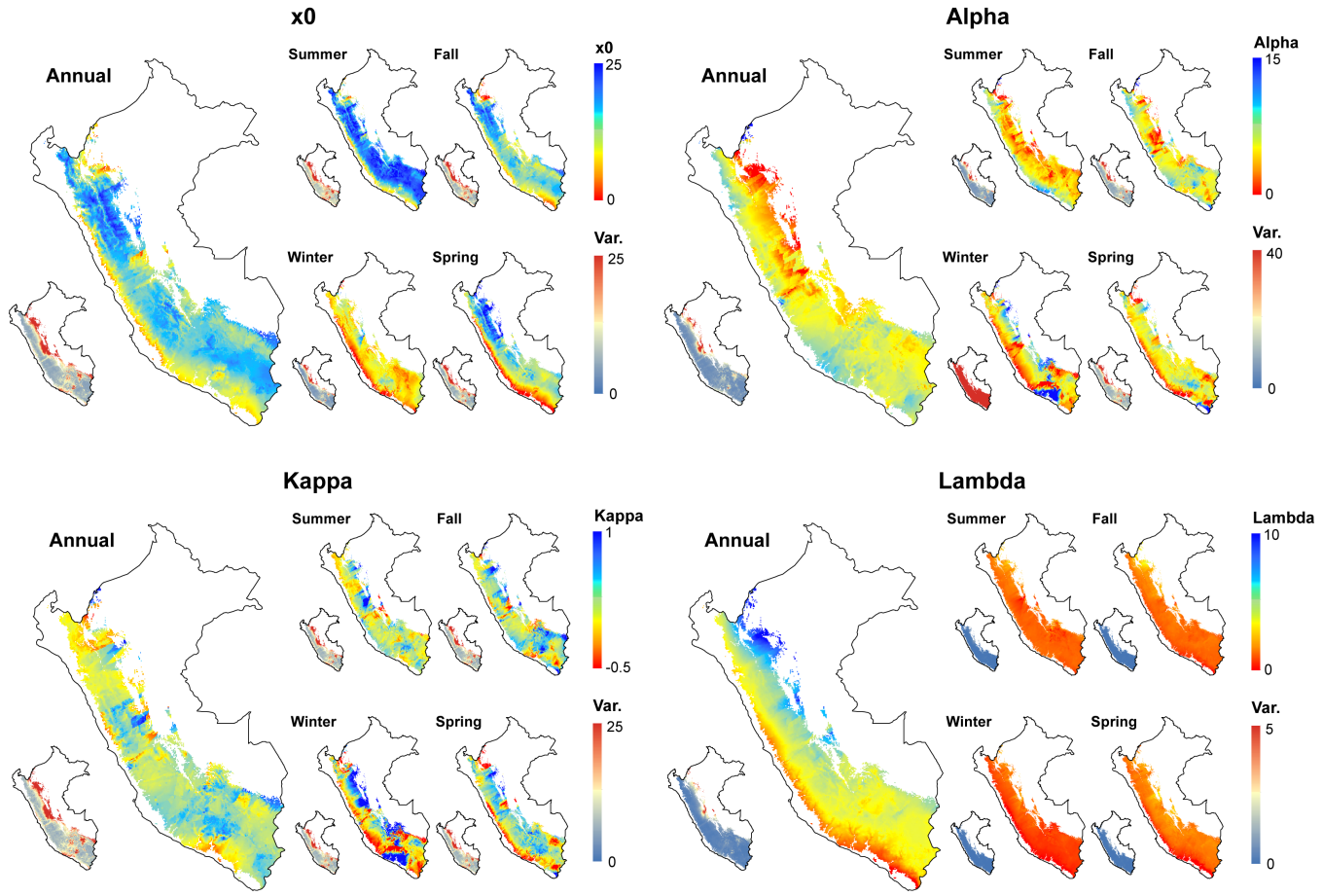

FIGURE 12 Spatial distribution of the annual and seasonal Generalized Pareto distribution parameters for precipitation intensity. Small maps represent the distribution of the variance obtained from the universal kriging models [Colour figure can be viewed at wileyonlinelibrary.com]

precipitation intensity, either for a period of 25 or 50 years, with a clear southwest-northeast gradient. The uncertainty of these estimates, as revealed by standard deviation values, suggests higher uncertainty in winter, particularly for north-eastern region of the Andes. This behaviour may be explained by the low data availability at this region.

Figure 14 indicates that maximum precipitation duration (days) shows more complex spatial patterns, with an expected higher maximum duration of wet events (>70 days) within a period of 50 years. This pattern is more pronounced over large areas of the Central and Southern Andes. This annual pattern is found for autumn season as well, but with higher uncertainty. On the contrary, the expected maximum precipitation duration is likely very low during winter and spring. This finding is confirmed, by the low standard deviation values found during these seasons. Spatially, the Northern Andes show low maximum duration of wet events at the annual and seasonal scales.

Maximum total precipitation magnitude during a wet event shows similar spatial patterns with the patterns found for precipitation duration (Figure 15), with the highest values recorded in the Central-South Andes. Spatially, the patterns at the annual scale also coincide with those of the autumn season. A higher variance and stronger spatial uncertainty of the estimations is recorded during summer.

Finally, the expected maximum dry-spell duration within a period of 50 years shows coherent spatial patterns (Figure 16), with higher values (>120 dry days) being found in the western slopes of the Andes. On the contrary, in the Central Andes, the maximum dry-spell length at the annual scale is lower than 30 days; which is spatially more related to the patterns found during cold and wet seasons (i.e., summer and spring seasons). Figure 16 also suggests higher uncertainty of dry-spell length estimations during spring.

Figure 17 plots the relationship between the on-site predicted precipitation variables for a period of 25 years using the GPA distribution and those predicted using the kriging universal models using the jackknife approach. Similar

TABLE 1 Mean weighted correlations and Willmott's *D* values obtained from the P–P plots and the different variables at annual and seasonal scales, averaged for the 178 meteorological stations

	Mean weighted correlation	***SD* weighted correlation**	**Mean *D***	***SD***
Intensity (annual)	0.999	0.001	0.999	0.001
Intensity (summer)	0.996	0.003	0.998	0.002
Intensity (autumn)	0.997	0.003	0.998	0.002
Intensity (winter)	0.993	0.007	0.952	0.178
Intensity (spring)	0.996	0.006	0.997	0.006
Duration (annual)	0.999	0.001	0.999	0.001
Duration (summer)	0.996	0.003	0.998	0.002
Duration (autumn)	0.996	0.003	0.997	0.002
Duration (winter)	0.992	0.005	0.907	0.233
Duration (spring)	0.996	0.003	0.969	0.145
Magnitude (annual)	0.998	0.001	0.999	0.001
Magnitude (summer)	0.995	0.003	0.997	0.002
Magnitude (autumn)	0.995	0.003	0.996	0.002
Magnitude (winter)	0.990	0.008	0.949	0.182
Magnitude (spring)	0.995	0.005	0.996	0.006
Dry spell length (annual)	0.997	0.003	0.997	0.003
Dry spell length (summer)	0.995	0.005	0.996	0.004
Dry spell length (autumn)	0.996	0.003	0.997	0.003
Dry spell length (winter)	0.989	0.010	0.941	0.208
Dry spell length (spring)	0.991	0.010	0.993	0.007

TABLE 2 Willmott's *D* accuracy measurement between on-site estimated parameters ($+\lambda$) and those obtained by spatial modelling

	x_0 *D*	α *D*	κ *D*	λ *D*
Intensity (annual)	0.83	0.64	0.62	0.9
Intensity (summer)	0.81	0.66	0.41	0.49
Intensity (autumn)	0.85	0.65	0.52	0.84
Intensity (winter)	0.82	0.33	0.35	0.83
Intensity (spring)	0.92	0.39	0.44	0.94
Duration (annual)	0.66	0.57	0.75	0.83
Duration (summer)	0.67	0.61	0.49	0.54
Duration (autumn)	0.6	0.52	0.6	0.76
Duration (winter)	0.64	0.48	0.49	0.77
Duration (spring)	0.72	0.73	0.36	0.88
Magnitude (annual)	0.77	0.46	0.83	0.92
Magnitude (summer)	0.74	0.48	0.5	0.54
Magnitude (autumn)	0.65	0.41	0.67	0.88
Magnitude (winter)	0.78	0.53	0.4	0.86
Magnitude (spring)	0.88	0.82	0.3	0.96
Dry spell length (annual)	0.92	0.85	0.81	0.92
Dry spell length (summer)	0.88	0.94	0.84	0.55
Dry spell length (autumn)	0.84	0.75	0.54	0.84
Dry spell length (winter)	0.92	0.57	0.34	0.83
Dry spell length (spring)	0.88	0.69	0.75	0.94

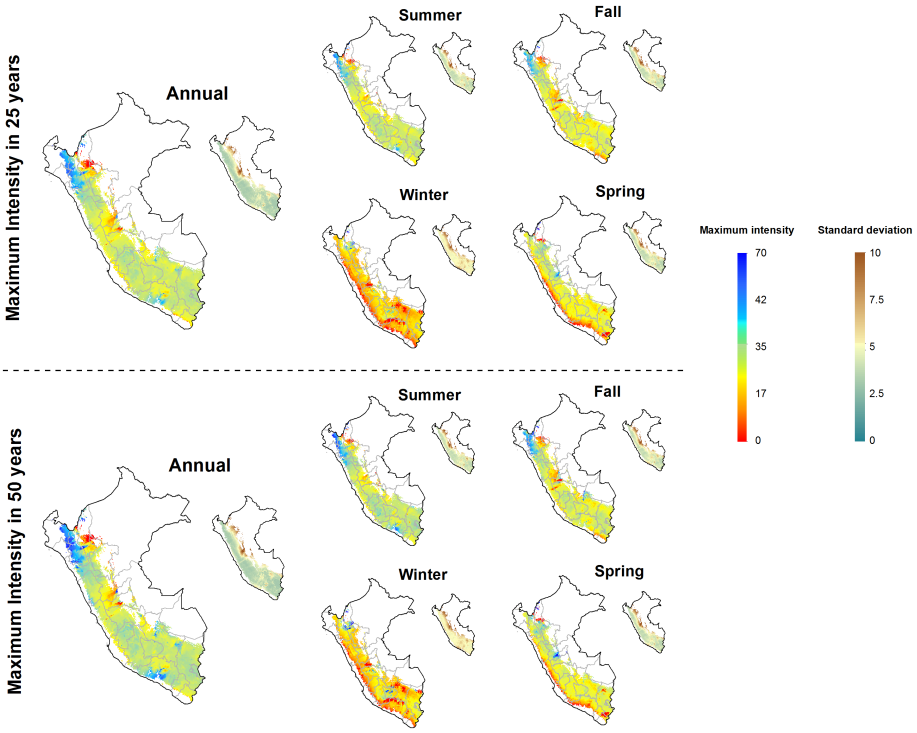

FIGURE 13 Spatial distribution of the expected annual and seasonal maximum precipitation intensity for a period of 25 and 50 years. Small maps represent one standard deviation of the estimation [Colour figure can be viewed at wileyonlinelibrary.com]

results are illustrated in Figure 56 in Appendix S1, but for an estimation period of 50 years.

Overall, there is a strong agreement between the precipitation intensity and dry spell length predicted using GPA distribution and those of kriging method. This agreement is lower for precipitation duration and magnitude. Nevertheless, there are important seasonal differences. In particular, precipitation duration estimated using kriging method for summer and spring, as well as precipitation magnitude estimations for winter and spring, show strong agreement with the GPA estimations. Table 3 summarizes the accuracy statistics obtained for the annual and seasonal

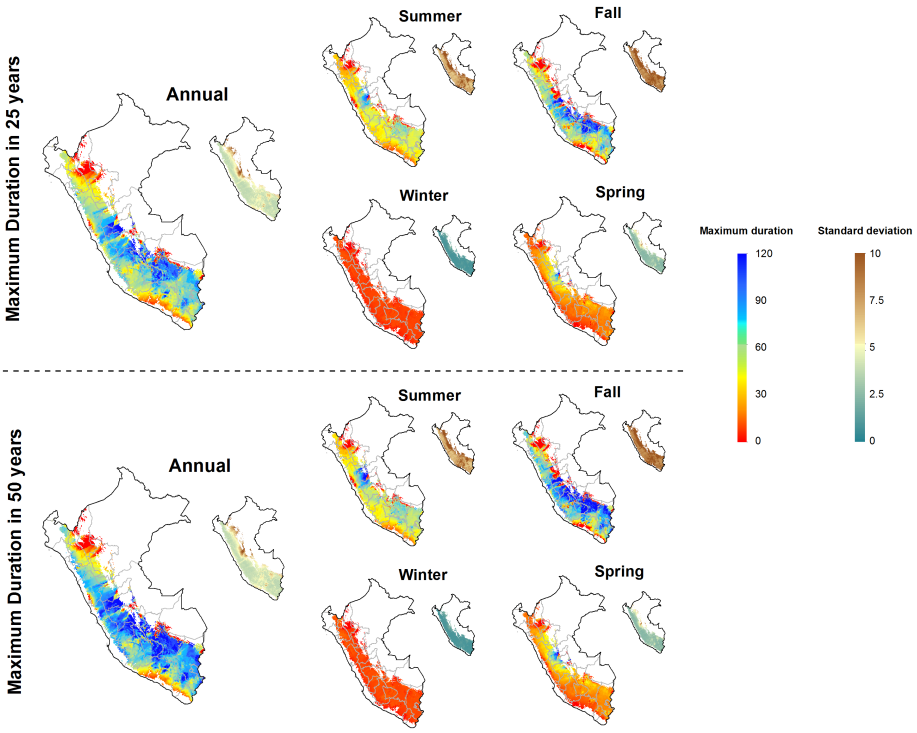

FIGURE 14 As Figure 13, but for maximum precipitation duration [Colour figure can be viewed at wileyonlinelibrary.com]

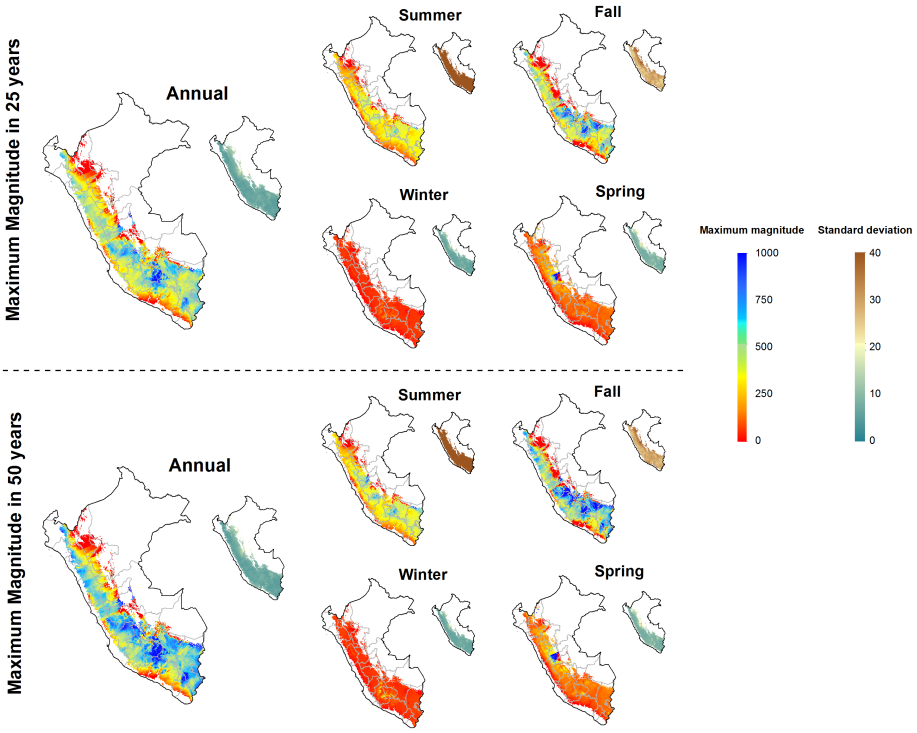

FIGURE 15 As Figure 13, but for maximum precipitation magnitude [Colour figure can be viewed at wileyonlinelibrary.com]

series of the four precipitation variables. Similar to many regions with complex topography, results stress the difficulty of an accurate mapping of precipitation hazard in the Peruvian Andes. The average spatial errors are important for some precipitation variables. Willmott's *D* agreement index provides good results, with values generally higher than 0.8, for rainfall intensity and dry spell length, but the agreement between the observed and estimated values is lower for precipitation duration and magnitude.

5 | DISCUSSION AND CONCLUSION

This study explains the methodology and results to generate for the first time precipitation hazard maps for the Peruvian

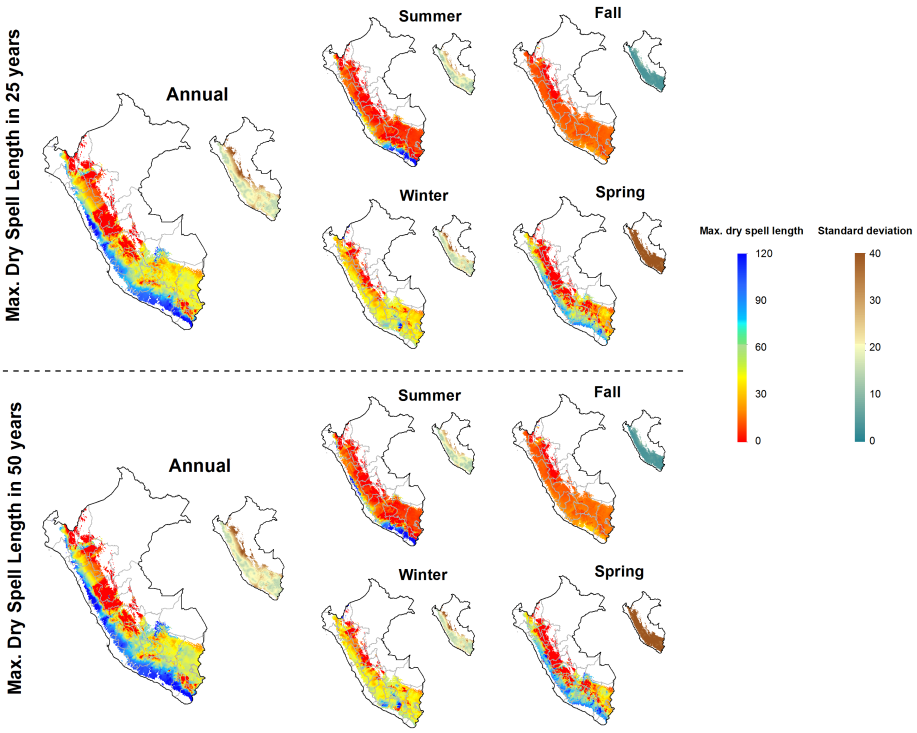

FIGURE 16 As Figure 13, but for maximum precipitation dry spell length [Colour figure can be viewed at wileyonlinelibrary.com]

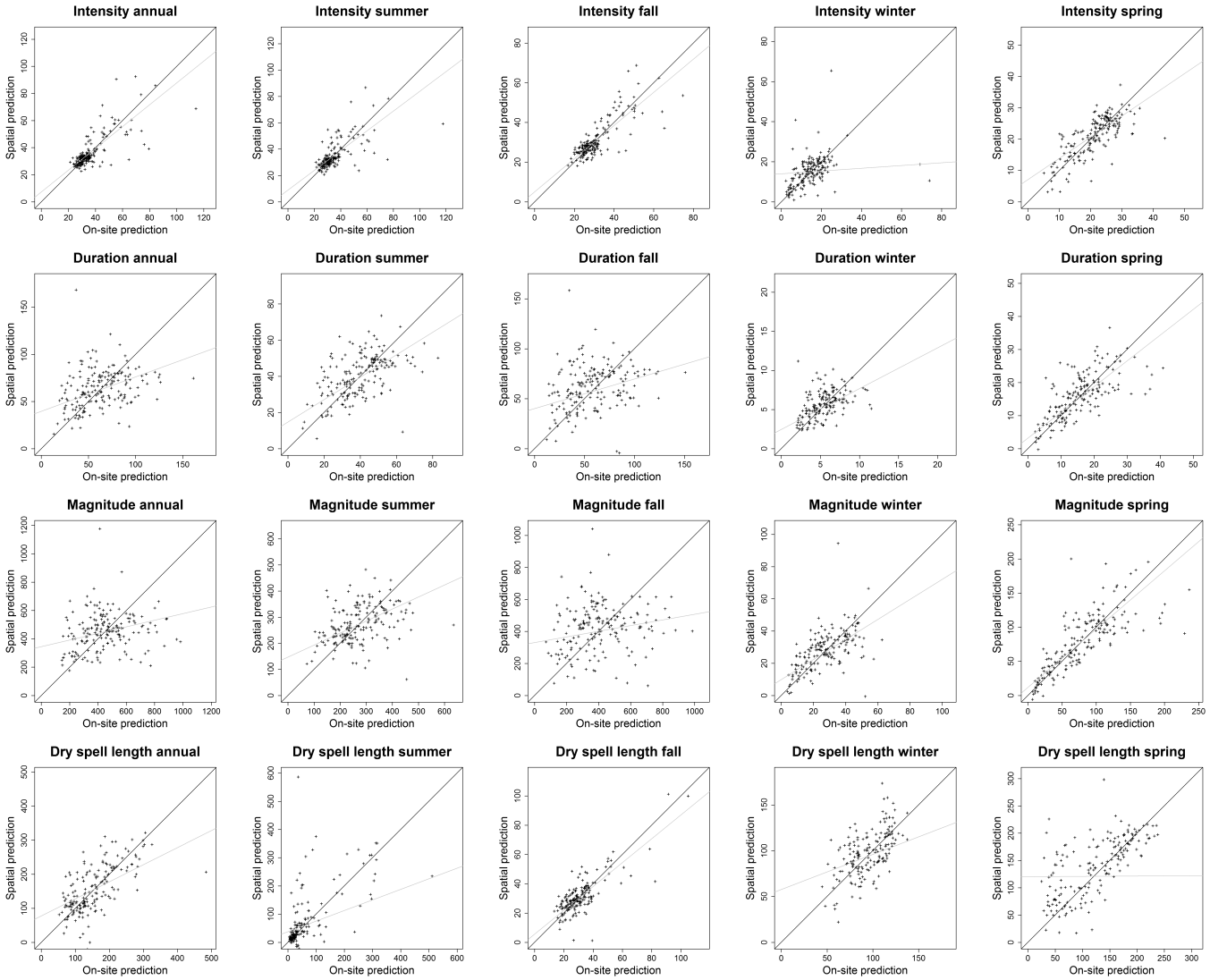

FIGURE 17 Relationship between the on-site estimation of the annual and seasonal maximum precipitation intensity, duration, magnitude and dry-spell length expected in a period of 25 years and the spatial prediction by means of the kriging universal models using the jack-knife approach

Andes. For this purpose, we followed an approach based on the Extreme Value Theory, merged with spatial mapping, employing the entire daily precipitation records available across Peru. The aim was to develop quantile maps for different daily precipitation variables at annual and seasonal scales, including: precipitation intensity, magnitude, duration, and dry-spell length. Probabilistic analyses were based on exceedance series for these four variables, considering different thresholds, which were fitted to a GPA distribution.

In agreement with previous studies in other regions (e.g., Madsen *et al.,* 1998; Lana *et al.,* 2006; Cooley *et al.,* 2007), we found that the exceedance series for the different daily precipitation variables show a general fit to the GPA distribution in the Peruvian Andes. This is clearly observed for the different annual and seasonal L-moment diagrams developed for precipitation variables. Nevertheless, we demonstrated that the selected threshold for the development of the exceedance series plays an important role in the distribution fitting and the quality of the estimations. Beguería (2005) and Vicente-Serrano and Beguería-Portugués (2003) confirmed that the threshold choice may produce important differences in the quantile estimates considering precipitation intensity and dry-spell length. Our results agree with these studies, given that estimations for the different daily precipitation variables in the Peruvian Andes showed better agreement between observed and predicted maximum precipitation intensity, duration, magnitude and dry spell length considering high centiles (>90th) as thresholds. Thus, lower precipitation thresholds (<80th centile) tend to clearly underestimate maximum estimated values for the four precipitation variables. Although it is challenging to choose the most suitable threshold, we considered the need of maintaining a balance between the goodness of estimations and the sample size (i.e., length of the series). Following our results as well as the recommendations of previous works (e.g., Beguería *et al.,* 2009; Babu and Toreti, 2016), we decided to choose the 90th centile as the most suitable threshold to develop the exceedance series. Thus, the quantile estimates by means of

TABLE 3 Accuracy statistics (*D*, MAE and weight *r*) between on-site estimation of the annual and seasonal maximum precipitation intensity, duration, magnitude and dry-spell length expected in a period of 25 and 50 years and the spatial prediction by means of the kriging universal models using the jack-knife approach

	Maximum in 25 years			Maximum in 50 years		
	D	**MAE**	**Weighted *r***	***D***	**MAE**	**Weighted *r***
Intensity (annual)	0.86	5.22	0.74	0.86	6.38	0.75
Intensity (summer)	0.80	5.11	0.65	0.81	6.68	0.67
Intensity (autumn)	0.90	3.82	0.80	0.89	4.58	0.79
Intensity (winter)	0.31	6.05	0.03	0.13	9.80	0.03
Intensity (spring)	0.82	3.72	0.59	0.73	4.46	0.42
Duration (annual)	0.56	20.78	0.23	0.54	26.31	0.19
Duration (summer)	0.73	9.38	0.46	0.71	11.00	0.44
Duration (autumn)	0.54	22.93	0.19	0.54	27.31	0.18
Duration (winter)	0.67	1.46	0.40	0.65	1.92	0.38
Duration (spring)	0.82	4.09	0.59	0.80	5.17	0.55
Magnitude (annual)	0.48	151.41	0.07	0.48	199.41	0.07
Magnitude (summer)	0.60	70.73	0.28	0.55	85.22	0.20
Magnitude (autumn)	0.46	170.80	0.05	0.46	213.67	0.07
Magnitude (winter)	0.76	8.21	0.40	0.65	11.55	0.23
Magnitude (spring)	0.88	20.53	0.64	0.85	26.25	0.58
Dry spell length (annual)	0.75	44.13	0.61	0.69	52.51	0.52
Dry spell length (summer)	0.69	47.80	0.64	0.61	64.07	0.56
Dry spell length (autumn)	0.88	5.64	0.85	0.88	7.29	0.83
Dry spell length (winter)	0.71	17.82	0.57	0.59	21.77	0.45
Dry spell length (spring)	0.03	113.19	0.13	0.02	247.45	0.09

the GPA distribution, considering the 90th centile as threshold, provide a very good agreement with the empirical quantiles, irrespective of precipitation variable and timescale (i.e., annual vs. seasonal).

The spatial mapping of GPA distribution parameters using the universal kriging method shows different results, as a function of precipitation variable, timescale (seasonal and annual) and the distribution parameter. In general, λ and ε show lower errors using the jack-knife methodology, compared to α and κ. Nevertheless, there are some exceptions, where we found a high agreement between observed and interpolated α and κ parameters for annual, summer and spring series.

In general, it is difficult to determine whether the estimates of κ differ significantly from zero for a given sample (Rosbjerg *et al.,* 1992) and thus some authors consider it as constant at the regional level (e.g., Beguería *et al.,* 2009; Sang and Gelfand, 2009; Carreau *et al.,* 2017). Nevertheless, some studies comparing the use of regional or locally estimated parameters to estimate maps of precipitation intensity do not provide clear advantages of using regionalized parameters (e.g., Mailhot *et al.,* 2013). The strong climate differences in the Peruvian Andes adds further difficulties to this regionalization, as climate shows strong variations over short distance due to topographical gradient (Vuille *et al.,* 2000; Garreaud, 2009; Garreaud *et al.,* 2009). Several studies confirmed the skill of local estimation of the GPA parameters, even for the more erratic shape parameter (e.g., Begueria and Vicente-Serrano, 2006; Blanchet and Lehning, 2010). Here, we confirmed that the capability of the spatial interpolation models to locally reproduce the GPA parameters depends largely on precipitation variable as well as the timescale. We must also consider that the mapping approach followed in this study is based on a low density meteorological network, which is uneven for a large and complex region characterized by several local climate features like the Andes. For this reason, it may be expected that a denser meteorological network in the region can lead to a significant improvement in the spatial mapping of the parameters obtained following the extreme value theory and the GPA distribution.

Nevertheless, independently of the difficulty of locally estimating the distribution parameters for some variables and periods, we found a general coherent spatial pattern of precipitation quantiles, based on the maximum values for the four variables at the annual and seasonal scales. Albeit with some uncertainty in mapping the different distribution parameters, we showed a reasonable agreement between the at-site estimated maximum values for the four precipitation variables and those obtained by the interpolation of the parameters for a period of 25 and 50 years. Thus, the spatial estimation of the seasonal and annual precipitation intensity and dry spell length can be considered satisfactory given the available information. For example, the MAE for the estimated maximum precipitation intensity is generally lower than 10 mm, which is low for a range that oscillates between 0 and 70 mm in a period of 50 years.

The maps obtained provide a useful general assessment of the spatial distribution of the precipitation hazard probability across the Peruvian Andes. To improve its dissemination among scientific community and stakeholders the maps of the annual and seasonal parameters of the four precipitation variables are available at https://digital.csic.es/.

ACKNOWLEDGEMENTS

This work was supported by the research projects PCIN-2015-220 and CGL2014-52135-C03-01 financed by the Spanish Commission of Science and Technology and FEDER, IMDROFLOOD financed by the Water Works 2014 co-funded call of the European Commission and INDECIS, financed by the ERA-NET Cofund for Climate Services of the European Research Area for Climate Services. Marina Peña-Gallardo was granted by the Spanish Ministry of Economy and Competitiveness and Miquel Tomas-Burguera and Francisco Navarro-Serrano were supported by a doctoral grant by the Spanish Ministry of Education, Culture and Sport.

REFERENCES

Alexandersson, H. (1986) A homogeneity test to precipitation data. *Journal of Climatology*, 6, 661–675.

Attorre, F., Alfo, M., De Sanctis, M., Francesconi, F. and Bruno, F. (2007) Comparison of interpolation methods for mapping climatic and bioclimatic variables at regional scale. *International Journal of Climatology*, 27(13), 1825–1843.

Babu, G.J. and Toreti, A. (2016) A goodness-of-fit test for heavy tailed distributions with unknown parameters and its application to simulated precipitation extremes in the Euro-Mediterranean region. *Journal of Statistical Planning and Inference*, 174, 11–19.

Barron, J., Rockström, J., Gichuki, F. and Hatibu, N. (2003) Dry spell analysis and maize yields for two semi-arid locations in east Africa. *Agricultural and Forest Meteorology*, 117(1–2), 23–37.

Beguería, S. (2005) Uncertainties in partial duration series modelling of extremes related to the choice of the threshold value. *Journal of Hydrology*, 303(1), 215–230.

Begueria, S. and Vicente-Serrano, S.M. (2006) Mapping the hazard of extreme rainfall by peaks-over-threshold extreme value analysis and spatial regression techniques. *Journal of Applied Meteorology and Climatology*, 45, 108–124.

Beguería, S., Vicente-Serrano, S.M., López-Moreno, J.I. and García-Ruiz, J.M. (2009) Annual and seasonal mapping of peak intensity, magnitude and duration of extreme precipitation events across a climatic gradient, North-east Iberian Peninsula. *International Journal of Climatology*, 29, 1759–1779.

Belachsen, I., Marra, F., Peleg, N. and Morin, E. (2017) Convective rainfall in a dry climate: relations with synoptic systems and flash-flood generation in the Dead Sea region. *Hydrology and Earth System Sciences*, 21(10), 5165–5180.

Bendix, J. (2004) Climate variability and extreme events in the Andes of Ecuador and Peru. *Geographische Rundschau*, 56, 10–16.

Bendix, A. and Bendix, J. (2006) Heavy rainfall episodes in Ecuador during El Niño events and associated regional atmospheric circulation and SST patterns. *Advances in Geosciences*, 6, 43–49.

Blanchet, J. and Lehning, M. (2010) Mapping snow depth return levels: smooth spatial modeling versus station interpolation. *Hydrol. EarthSyst. Sci.*, 14(12), 2527–2544.

Boessenkool, B., Bürger, G. and Heistermann, M. (2017) Effects of sample size on estimation of rainfall extremes at high temperatures. *Natural Hazards and Earth System Sciences*, 17(9), 1623.

Borga, M., Boscolo, P., Zanon, F. and Sangati, M. (2007) Hydrometeorological analysis of the 29 August 2003 flash flood in the eastern Italian Alps. *Journal of Hydrometeorology*, 8(5), 1049–1067.

Burrough, P.A. and McDonnell, R.A. (1998) *Principles of Geographic Information Systems*. Oxford, UK: Oxford University Press.

Carreau, J., Naveau, P. and Neppel, L. (2017) Partitioning into hazard subregions for regional peaks-over-threshold modeling of heavy precipitation. *Water Resources Research*, 53(5), 4407–4426.

Coles, S. (2001) *An Introduction to Statistical Modeling of Extreme Values*. London, UK: Springer.

Cooley, D., Nychka, D. and Naveau, P. (2007) Bayesian spatial modeling of extreme precipitation return levels. *Journal of the American Statistical Association*, 102(479), 824–840.

Crosta, G. (1998) Regionalization of rainfall thresholds: an aid to landslide hazard evaluation. *Environmental Geology*, 35(2–3), 131–145.

Daly, C., Neilson, R.P. and Phillips, D.L. (1994) A statistical-topographic model for mapping climatological precipitation over mountainous terrain. *Journal of applied meteorology*, 33(2), 140–158.

Dullo, T.T., Kalyanapu, A.J. and Teegavarapu, R.S.V. (2017) Evaluation of changing characteristics of temporal rainfall distribution within 24-hour duration storms and their influences on peak discharges: case study of Asheville, North Carolina. *Journal of Hydrologic Engineering*, 22(11), 05017022.

Easterling, D.R. and Peterson, T.C. (1995) A new method of detecting undocumented discontinuities in climatological time series. *International Journal of Climatology*, 15, 369–377.

El Kenawy, A., Lopez-Moreno, J.I., Vicente-Serrano, S.M. and Morsi, F. (2010) Climatological modeling of monthly air temperature and precipitation in Egypt through GIS techniques. *Climate Research*, 42(2), 161–176.

Esteves, L.S. (2013) Consequences to flood management of using different probability distributions to estimate extreme rainfall. *Journal of Environmental Management*, 115, 98–105.

Fitzgerald, D.L. (1989) Single station and regional analysis of daily rainfall extremes. *Stochastic Hydrology and Hydraulics*, 3(4), 281–292.

Garreaud, R.D. (2009) The Andes climate and weather. *Advances in Geosciences*, 22, 3–11.

Garreaud, R.D., Vuille, M., Compagnucci, R. and Marengo, J. (2009) Present-day South American climate. *Palaeogeography, Palaeoclimatology, Palaeoecology*, 281(3–4), 180–195.

Grimm, A.M. and Tedeschi, R.G. (2009) ENSO and extreme rainfall events in South America. *Journal of Climate*, 22(7), 1589–1609.

Haagenson, E.C. (2012) *Statistical Methods for Water Demand Modeling to Help Mitigate Climate Induced Risk*. Boulder: University of Colorado.

Halder, D., Panda, R.K., Srivastava, R.K., Kheroar, S. and Singh, S.P. (2016) Stochastic analysis of rainfall and its application in appropriate planning and management for Eastern India agriculture. *Water Policy*, 18(5), 1155–1173.

Haylock, M.R., Peterson, T.C., Alves, L.M., Ambrizzi, T., Anunciação, Y.M.T., Baez, J., Barros, V.R., Berlato, M.A., Bidegain, M., Coronel, G., Corradi, V., Garcia, V.J., Grimm, A.M., Karoly, D., Marengo, J.A., Marino, M.B., Moncunill, D.F., Nechet, D., Quintana, J., Rebello, E., Rusticucci, M., Santos, J.L., Trebejo, I. and Vincent, L.A. (2006) Trends in total and extreme South American rainfall in 1960-2000 and links with sea surface temperature. *Journal of Climate*, 19(8), 1490–1512.

Hofstra, N., Haylock, M., New, M., Jones, P. and Frei, C. (2008) Comparison of six methods for the interpolation of daily, European climate data. *Journal of Geophysical Research Atmospheres*, 113(21), D21110.

Holdaway, M.R. (1996) Spatial modeling and interpolation of monthly temperature using kriging. *Climate Research*, 6, 215–225.

Hosking, J.R.M. (1990) L-moments: analysis and estimation of distributions using linear combinations of order statistics. *Journal of the Royal Statistical Society Series B: Methodological*, 52, 105–124.

Hosking, J.R.M. and Wallis, J.R. (1987) Parameter and quantile estimation for the generalized Pareto distribution. *Technometrics*, 29, 339–349.

Hosking, J.R.M. and Wallis, J.R. (2005) *Regional Frequency Analysis: An Approach Based on l-Moments*. Cambridge, UK: Cambridge University Press.

Houston, J. (2006) The great Atacama flood of 2001 and its implications for Andean hydrology. *Hydrological Processes*, 20, 591–610.

Kane, R.P. (1999) Rainfall extremes in some selected parts of Central and South America: ENSO and other relationships reexamined. *International Journal of Climatology*, 19, 423–455.

Lana, X., Burgueño, A., Martínez, M.D. and Serra, C. (2006) Statistical distributions and sampling strategies for the analysis of extreme dry spells in Catalonia (NE Spain). *Journal of Hydrology*, 324(1–4), 94–114.

Lavado Casimiro, W.S., Labat, D., Ronchail, J., Espinoza, J.C. and Guyot, J.L. (2013) Trends in rainfall and temperature in the Peruvian Amazon-Andes basin over the last 40years (1965-2007). *Hydrological Processes*, 27(20), 2944–2957.

Lawrence, J., Reisinger, A., Mullan, B. and Jackson, B. (2013) Exploring climate change uncertainties to support adaptive management of changing flood-risk. *Environmental Science and Policy*, 33, 133–142.

Madsen, H., Rosbjerg, D. and Harremoes, P. (1994) PDS-modelling and regional Bayesian estimation of extreme rainfalls. *Nordic Hydrology*, 25(4), 279–300.

Madsen, H., Mikkelsen, P.S., Rosbjerg, D. and Harremoes, P. (1998) Estimation of regional intensity-duration-frequency curves for extreme precipitation. *Water Science and Technology*, 37(11), 29–36.

Madsen, H., Gregersen, I.B., Rosbjerg, D. and Arnbjerg-Nielsen, K. (2017) Regional frequency analysis of short duration rainfall extremes using gridded daily rainfall data as co-variate. *Water Science and Technology*, 75, 1971–1981.

Mailhot, A., Lachance-Cloutier, S., Talbot, G. and Favre, A.C. (2013) Regional estimates of intense rainfall based on the Peak-Over-Threshold (POT) approach. *Journal of hydrology*, 476, 188–199.

Naveau, P., Toreti, A., Smith, I. and Xoplaki, E. (2014) A fast nonparametric spatio-temporal regression scheme for generalized Pareto distributed heavy precipitation. *Water Resour. Res.*, 50, 4011–4017.

Panthou, G., Vischel, T., Lebel, T., et al. (2015) Mapping rainfall return level in West Africa: comparison of different approaches. *Houille Blanche*, 6, 42–48.

Papalexiou, S.M., Koutsoyiannis, D. and Makropoulos, C. (2013) How extreme is extreme? An assessment of daily rainfall distribution tails. *Hydrol. Earth Syst. Sci.*, 17(2), 851–862.

Pebesma, E.J. (2004) Multivariable geostatistics in S: the gstat package. *Comput. Geosci.*, 30, 683–691.

Pham, H.X., Asaad, Y. and Melville, B. (2014) Statistical properties of partial duration series: case study of North Island, New Zealand. *Journal of Hydrologic Engineering*, 19(4), 807–815.

Phillips, D.L., Dolph, J. and Marks, D. (1992) A comparison of geostatistical procedures for spatial analysis of precipitation in mountainous terrain. *Agricultural and Forest Meteorology*, 58(1–2), 119–141.

Rosbjerg, D., Madsen, H. and Rasmussen, P.F. (1992) Prediction in partial duration series with generalized Pareto-distributed exceedances. *Water Resources Research*, 28(11), 3001–3010.

Saharia, M., Kirstetter, P.E., Vergara, H., Gourley, J.J. and Hong, Y. (2017) Characterization of floods in the United States. *Journal of Hydrology*, 548, 524–535.

Sang, H. and Gelfand, A.E. (2009) Hierarchical modeling for extreme values observed over space and time. *Environ. Ecol. Stat.*, 16(3), 407–426.

Seiler, C., Hutjes, R.W.A. and Kabat, P. (2013) Climate variability and trends in Bolivia. *Journal of Applied Meteorology and Climatology*, 52, 130–146.

Serinaldi, F. and Kilsby, C.G. (2014) Simulating daily rainfall fields over large areas for collective risk estimation. *Journal of Hydrology*, 512, 285–302.

Serra, C., Lana, X., Burgueño, A. and Martínez, M.D. (2016) Partial duration series distributions of the European dry spell lengths for the second half of the twentieth century. *Theoretical and Applied Climatology*, 123(1–2), 63–81.

She, D., Xia, J., Song, J., du, H., Chen, J. and Wan, L. (2013) Spatio-temporal variation and statistical characteristic of extreme dry spell in Yellow River basin, China. *Theoretical and Applied Climatology*, 112(1–2), 201–213.

Sheng, J. and Zwiers, F. (1998) An improved scheme for time-dependent boundary conditions in atmospheric general circulation models. *Climate Dynamics*, 14, 609–613.

Skansi, M.D.L.M., Brunet, M., Sigró, J., Aguilar, E., Arevalo Groening, J.A., Bentancur, O.J., Castellón Geier, Y.R., Correa Amaya, R.L., Jácome, H., Malheiros Ramos, A., Oria Rojas, C., Max Pasten, A., Sallons Mitro, S., Villaroel Jiménez, C., Martínez, R., Alexander, L.V. and Jones, P.D. (2013) Warming and wetting signals emerging from analysis of changes in climate extreme indices over South America. *Global and Planetary Change*, 100, 295–307.

Sulca, J., Takahashi, K., Espinoza, J.C., Vuille, M. and Lavado-Casimiro, W. (2017) Impacts of different ENSO flavors and tropical Pacific convection variability (ITCZ, SPCZ) on austral summer rainfall in South America, with a focus on Peru. *International Journal of Climatology.*, 38, 420–435. https://doi.org/10.1002/joc.5185.

Szolgay, J., Parajka, J., Kohnová, S., et al. (2007) Testing of mapping approaches for estimation of 100-year maximum daily precipitation totals in the upper Hron River basin. *Geophysics and Geodesy*, 37(3), 225–246.

Szolgay, J., Parajka, J., Kohnová, S. and Hlavčová, K. (2009) Comparison of mapping approaches of design annual maximum daily precipitation. *Atmospheric Research*, 92(3), 289–307.

Tramblay, Y., Neppel, L., Carreau, J. and Najib, K. (2013) Non-stationary frequency analysis of heavy rainfall events in southern France. *Hydrological Sciences Journal*, 58(2), 280–294.

Trefry, C.M., Watkins, D.W., Jr. and Johnson, D. (2005) Regional rainfall frequency analysis for the state of Michigan. *Journal of Hydrologic Engineering*, 10(6), 437–449.

Vicente-Serrano, S.M. and Beguería-Portugués, S. (2003) Estimating extreme dry-spell risk in the middle Ebro valley (northeastern Spain): a comparative analysis of partial duration series with a general Pareto distribution and annual maxima series with a Gumbel distribution. *International Journal of Climatology*, 23(9), 1103–1118.

Vicente-Serrano, S.M., Sánchez, S. and Cuadrat, J.M. (2003) Comparative analysis of interpolation methods in the middle Ebro Valley (Spain): application to annual precipitation and temperature. *Climate Research*, 24(2), 161–180.

Vicente-Serrano, S.M., Beguería, S., López-Moreno, J.I., El Kenawy, A.M. and Angulo-Martínez, M. (2009) Daily atmospheric circulation events and extreme precipitation risk in northeast Spain: Role of the North Atlantic Oscillation, the Western Mediterranean Oscillation, and the Mediterranean Oscillation. *Journal of Geophysical Research: Atmospheres*, 114, D08106.

Vicente-Serrano, S.M., Aguilar, E., Martínez, R., Martín-Hernández, N., Azorin-Molina, C., Sanchez-Lorenzo, A., El Kenawy, A., Tomás-Burguera, M., Moran-Tejeda, E., López-Moreno, J.I., Revuelto, J., Beguería, S., Nieto, J.J., Drumond, A., Gimeno, L. and Nieto, R. (2017) The complex influence of ENSO on droughts in Ecuador. *Climate Dynamic*, 48(1–2), 405–427.

Vilímek, V., Klimeš, J., Vlcko, J. and Carreño, R. (2006) Catastrophic debris flows near Machu Picchu village (Aguas Calientes), Peru. *Environmental Geology*, 50, 1041–1052.

Vincen, L. (1998) A technique for the identification of inhomogeneities in Canadian temperature series. *Journal of Climate*, 11, 1094–1104.

Vuille, M., Bradley, R.S. and Keimig, F. (2000) Interannual climate variability in the Central Andes and its relation to tropical Pacific and Atlantic forcing. *Journal of Geophysical Research Atmospheres*, 105(D10), 12447–12460.

Wang, Q.J. (1991) The POT model described by the generalized Pareto distribution with Poisson arrival rate. *Journal of Hydrology*, 129(1–4), 263–280.

Weisse, A.K. and Bois, P. (2002) A comparison of methods for mapping statistical characteristics of heavy rainfall in the French Alps: the use of daily information. *Hydrological Sciences Journal*, 47(5), 739–752.

Willmott, C.J. (1981) On the validation of models. *Physical Geography*, 2(2), 184–194.

Yarleque, C., Vuille, M., Hardy, D.R., Posadas, A. and Quiroz, R. (2016) Multiscale assessment of spatial precipitation variability over complex mountain terrain using a high-resolution spatiotemporal wavelet reconstruction method. *J. Geophys. Res. Atmos.*, 121, 12,198–12,216.

SUPPORTING INFORMATION

Additional supporting information may be found online in the Supporting Information section at the end of the article.

How to cite this article: Domínguez-Castro F, Vicente-Serrano SM, López-Moreno JI, *et al.* Mapping seasonal and annual extreme precipitation over the Peruvian Andes. *Int J Climatol*. 2018;1–17. https://doi.org/10.1002/joc.5739